Temporal Coupled-Mode Theory for Fano Resonance in Light Scattering by a Single Obstacle†

Zhichao Ruan and Shanhui Fan*

Ginzton Laboratory, Department of Electrical Engineering, Stanford University, Stanford, California 94305

Received: September 16, 2009; Revised Manuscript Received: November 17, 2009

We present a theory for Fano interference in light scattering by individual obstacle, based on a temporal coupled-mode formalism. This theory is applicable for obstacles that are much smaller than the incident wavelength, or for systems with two-dimensional cylindrical or three-dimensional spherical symmetry. We show that for each angle momentum channel, the Fano interference effect can be modeled by a simple temporal coupled-mode equation, which provides a line shape formula for scattering and absorption cross-section. We validate the analysis with numerical simulations. As an application of the theory, we design a structure that exhibits strong absorption and weak scattering properties at the same frequency.

I. Introduction

Understanding light scattering by individual particles is of fundamental importance.[1] In recent years, the Fano interference effect[2] in such light scattering has attracted significant attention. Individual particles can support resonances. In the vicinity of such resonances, the spectrum of either scattering cross-section or extinction cross-section can exhibit a Fano line shape, where the spectrum varies asymmetrically with respect to resonant frequency.[3–8] Such Fano interference effects are also closely related to the classical analogue to electromagnetically induced transparency (EIT),[9] which have recently been proposed and demonstrated in scattering systems consisting of metallic elements.[10–16] Although the Fano effect in particle scattering has been demonstrated in different systems, given the ubiquitous nature of such an effect, it would be very useful to present a broader theory that captures some of general aspects.

In this paper, we generalize the temporal coupled-mode theory—previously developed to account for the Fano interference effect in waveguide or grating systems[17]—to treat light scattering by individual resonant obstacles. In the theory of ref 17, the Fano line shape appears in the transmission spectrum of the system. For an individual obstacle, the transmission spectrum is no longer well-defined. Instead, the theory here aims to calculate the scattering cross-section of the obstacle. Also related to this work, the temporal coupled mode theory has recently been generalized to treat small particle scattering in ref 18. The work of ref 18, however, did not include the Fano interference effect.

The paper is organized as follows: In section II, we show that for each angle momentum channel, the Fano interference effect can be modeled by a simple temporal coupled-mode equation, which provides a line shape formula for scattering and absorption cross-section. In section III, we compare the theoretical predictions to numerical simulations. Finally, in section IV, as an application of the theory, we design a structure that exhibits strong absorption and weak scattering properties at the same frequency.

† Part of the "Martin Moskovits Festschrift".

II. Theory

A. Brief Review of Standard Scattering Theory. We start by briefly reviewing the standard scattering theory for a single obstacle. For simplicity, this paper only discusses the two-dimensional (2D) case where the obstacle is uniform in the z direction, but the concept is straightforwardly generalizable to the three-dimensional cases. Consider an obstacle located at the origin, surrounding by air. When a TM wave (with its magnetic field H polarized along the z-direction) impinges on the obstacle, the total field in the air region outside the scatterer can be written as

$$H_{\text{total}} = \sum_{l=-\infty}^{\infty} H_0(h_l^+ H_l^{(2)}(k\rho)\exp(\mathrm{i}l\theta) + h_l^- H_l^{(1)}(k\rho)\exp(\mathrm{i}l\theta)) \tag{1}$$

where H_0 is a normalization constant, (ρ, θ) is the polar coordinates oriented at the origin, k is the wavenumber in air, and $H_l^{(1)}$ ($H_l^{(2)}$) is the lth order Hankel function of the first (second) kind. Since $H_l^{(1,2)}(k\rho) \rightarrow (2/\pi k)^{1/2} e^{\mathrm{i}[(l\pi/2)+(\pi/4)]} e^{(+,-)\mathrm{i}k\rho}/\rho^{1/2}$ when $\rho \rightarrow \infty$, and taking the convention that the field varies in time as $\exp(-\mathrm{i}\omega t)$, one can identify h_l^+ and h_l^- as the incoming and outgoing wave amplitudes. The power carried in such incoming (or outgoing) wave is

$$P_l^{\pm} = \frac{2}{\omega\varepsilon_0}|H_0|^2|h_l^{\pm}|^2 \tag{2}$$

(Notice that the power in two-dimension has the unit of W/m.) By choosing the magnetic field normalization

$$H_0 = 1\sqrt{\frac{W}{m}\frac{\omega\varepsilon_0}{2}} \tag{3}$$

we have then $|h_l^+|^2$ and $|h_l^-|^2$ representing the incoming and outgoing power carried by waves in the lth angular momentum channel, measured in the unit of W/m.

In the cases where the scatterer is much smaller than the incident wavelength, or the system has cylindrical symmetry, the lth order incoming wave only excites the same order outgoing wave. So we define R_l as

10.1021/jp9089722
Published on Web 12/11/2009

$$R_l \equiv \frac{h_l^-}{h_l^+} \tag{4}$$

which can be thought of as a "reflection coefficient" since it relates the outgoing wave to the incoming wave in each channel. Moreover, if the obstacle is lossless, the power carried by the outgoing wave must be equal to that of the incoming wave. Consequently,

$$R_l = e^{i\phi_l} \tag{5}$$

where ϕ_l is a real phase factor.

We will now calculate the scattering, absorption, and extinction cross-sections of an obstacle. For this purpose, imagining a plane wave incident upon the obstacle, the scattering (absorption) cross-section is then defined as the total power scattered (absorbed), divided by the intensity of the incident field. For 2D system the cross-section has the unit of length. Mathematically, for this scenario, we write the total field in the air region outside the scatterer as

$$H_{total} = H_0(\exp(i\mathbf{k}\cdot\mathbf{r}) + \sum_{l=-\infty}^{\infty} i^l S_l H_l^{(1)}(k\rho)\exp(il\theta)) \tag{6}$$

where $\mathbf{k}$ is the wave vector of the incident plane wave and S_l is related to the scattered field and referred to as the scattering coefficient. To connect to eq 1, the plane wave is expanded as

$$\exp(i\mathbf{k}\cdot\mathbf{r}) = \sum_{l=-\infty}^{\infty} i^l \frac{1}{2}(H_l^{(1)}(k\rho) + H_l^{(2)}(k\rho))\exp(il\theta) \tag{7}$$

Combining eqs 6 and 7, and comparing to eq 1, we have

$$S_l = \frac{R_l - 1}{2} \tag{8}$$

Furthermore, in the lth channel, the scattered power P_{sct} and the absorbed power P_{abs} are

$$P_{sct} = \frac{2}{\omega\varepsilon_0}|S_l|^2|H_0|^2$$
$$P_{abs} = \frac{1}{\omega\varepsilon_0}(1 - |R_l|^2)|H_0|^2 = \frac{2}{\omega\varepsilon_0}(-\mathrm{Re}\{S_l\} - |S_l|^2)|H_0|^2 \tag{9}$$

Following the definition of the scattering cross-section, the contribution to the total scattering cross-section from the lth channel is

$$C_{sct,l} \equiv \frac{P_{sct}}{I_0} = \frac{\frac{2}{\omega\varepsilon_0}|S_l|^2|H_0|^2}{\frac{1}{2}\sqrt{\frac{\mu_0}{\varepsilon_0}}|H_0|^2} = \frac{2\lambda}{\pi}|S_l|^2 \tag{10}$$

and the total scattering cross-section is

$$C_{sct} = \frac{2\lambda}{\pi}\sum_{l=-\infty}^{\infty}|S_l|^2 \tag{11}$$

where λ is the wavelength in air. In the same way, we have the total absorption cross-section as

$$C_{abs} = -\frac{2\lambda}{\pi}\sum_{l=-\infty}^{\infty}(\mathrm{Re}\{S_l\} + |S_l|^2) \tag{12}$$

Finally, the total extinction cross-section, as the sum of the scattering cross-section and the absorption cross-section, is

$$C_{ext} = -\frac{2\lambda}{\pi}\sum_{l=-\infty}^{\infty}\mathrm{Re}\{S_l\} \tag{13}$$

B. Coupled Mode Theory for Light Scattering. The goal of our theory is then to provide a general view about these cross-sections. In the following we consider the case that the obstacle supports resonance for the lth channel. In this circumstance, the Fano effect is the result of interference of two pathways: the direct "reflectance" of the incoming wave that forms the background, and the outgoing radiation from the excited resonance. Using the temporal coupled-mode theory formalism,[17–19] the dynamic equation for the amplitude c of the resonance is

$$\frac{dc}{dt} = (-i\omega_0 - \gamma_0 - \gamma)c + \kappa h^+$$
$$h^- = Bh^+ + \eta c \tag{14}$$

where ω_0 is the resonant frequency, γ_0 is the intrinsic loss rate due to for example material absorption, γ is the external leakage rate due to the coupling of the resonance to the outgoing wave, B is the background reflection coefficient, and κ and η correspond to the coupling constant between the resonance and the incoming or outgoing wave, respectively. In this section, as we consider only the lth channel, for notation simplicity we suppress the subscript l in all variables in eq 14. Here the amplitude c is normalized such that $|c|^2$ corresponds to the energy inside the resonator.[19] Note that such coupled-mode formalism is, strictly speaking, valid only when $\gamma_0 + \gamma \ll \omega_0$.[19]

The coupling constants κ and η are related to each other by energy conservation and time-reversal symmetry considerations.[17] In the lossless case (i.e., $\gamma_0 = 0$), if the incoming wave is absent (i.e., $h^+ = 0$), from eq 14 we have

$$c = A\exp(-i\omega_0 t - \gamma t)$$
$$h^- = A\eta\exp(-i\omega_0 t - \gamma t) \tag{15}$$

where A is an arbitrary constant. According to energy conservation, the energy leakage rate must be equal to the power of the outgoing wave, i.e.

$$\frac{d|c|^2}{dt} = -2\gamma|c|^2 = -|h^-|^2 = -\eta\eta^*|c|^2 \tag{16}$$

which requires that

$$\eta\eta^* = 2\gamma \tag{17}$$

Now let us perform a time-reversal transformation for the exponential decay process as described by eq 15. The time-reversed case is represented by feeding the resonator with exponentially growing wave amplitude $(h^-(-t))^*$. Such excitation results in a resonant amplitude $(c(-t))^*$ that also grows exponentially, without the outgoing wave. Described this time-reversed scenario using eq 14, we have

$$\kappa\eta^* = 2\gamma \tag{18a}$$
$$B\eta^* + \eta = 0 \tag{18b}$$

Comparing eq 18a to eq 17, we obtain

$$\kappa = \eta \tag{19}$$

Equations 17−19 are the main results of the Fano interference theory. If the system is lossless, the background reflection is $B = e^{i\phi}$ and therefore we can determine κ and η as

$$\kappa = \eta = \sqrt{2\gamma}e^{i(\phi/2+\pi/2-n\pi)} \tag{20}$$

where n is an arbitrary integer. For lossy systems, one should expect that the strongest contribution of the loss is to the resonant properties. In such a case, as an ansatz, we will introduce a nonzero intrinsic loss rate γ_0 in eq 14, while still approximating the background scattering as a lossless process. We will see below in the numerical example that such an approach is in fact sufficient for scattering from lossy plasmonic particles. A more rigorous approach, which we will not pursue here, will be to treat explicitly the loss as coupling to an additional decay channel, the combined system with the additional decay channel can then be treated using theory that is similar to eq 14 but without the need of introducing the intrinsic loss rate.

We now suppose that the incident wave has a frequency ω. The reflection coefficient R can be straightforwardly obtained using eqs 14 and 20:

$$\begin{aligned} R &= \frac{h^-}{h^+} = e^{i\phi} + \frac{-2\gamma e^{i\phi}}{i(\omega_0 - \omega) + \gamma_0 + \gamma} \\ &= \frac{i(\omega_0 - \omega) + \gamma_0 - \gamma}{i(\omega_0 - \omega) + \gamma_0 + \gamma} e^{i\phi} \end{aligned} \tag{21}$$

One can easily identify that in the lossless case (i.e., $\gamma_0 = 0$), the amplitude of R is unity, as expected. Following eq 8, the scattering coefficient is

$$\begin{aligned} S &= \frac{1}{2}(R - 1) \\ &= \frac{1}{2}\frac{(i(\omega_0 - \omega) + \gamma_0)(e^{i\phi} - 1) - \gamma(1 + e^{i\phi})}{i(\omega_0 - \omega) + \gamma_0 + \gamma} \end{aligned} \tag{22}$$

Substituting eqs 22 into eqs 11 and 12, we have the scattering and the absorption cross-sections as

$$C_{sct} = \frac{2\lambda}{\pi}\left|\frac{1}{2}\frac{(i(\omega_0 - \omega) + \gamma_0)(e^{i\phi} - 1) - \gamma(1 + e^{i\phi})}{i(\omega_0 - \omega) + \gamma_0 + \gamma}\right|^2 \tag{23a}$$

$$C_{abs} = \frac{2\lambda}{\pi}\frac{\gamma_0\gamma}{(\omega - \omega_0)^2 + (\gamma_0 + \gamma)^2} \tag{23b}$$

C. General Line Shapes in a Single Channel. We now use eq 23 to illustrate general line shapes of scattering and absorption cross-section spectra in a single channel. Let us first discuss the scattering cross-section. In the lossless case where $\gamma_0 = 0$, Figure 1 plots the scattering cross-section spectra with different phase factor ϕ as arised from the background "reflection".

For the phase factor $\phi = 0$, the spectrum is a Lorentzian function (Figure 1a). Note that the resonance creates maximal scattering at the resonant frequency ω_0. Since $\phi = 0$ corresponds to a very weak background scattering, in this case the only contribution to the scattering process is from the resonance. An example of a very weak background scattering is that for the H-polarization, as we consider here, when the radius of a metallic cylinder is far smaller than the wavelength. In this case, the presence of a surface-plasmon resonance would create a Lorenztian line shape in the scattering cross-section spectrum, and dramatically increase the scattering cross-section.

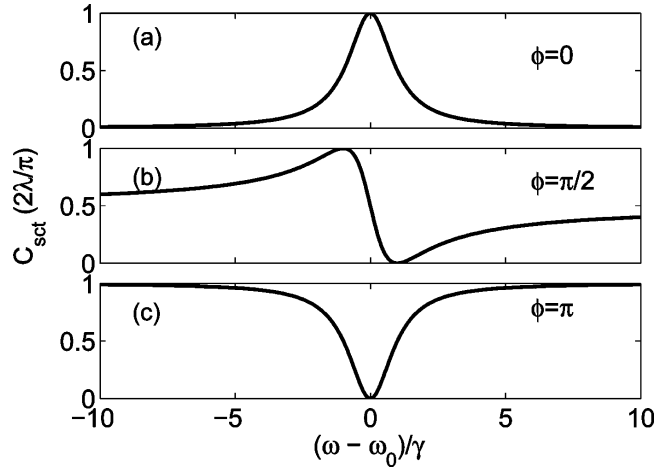

Figure 1. Scattering cross-section spectrum as given by eq 23 for the lossless case ($\gamma_0 = 0$). (a)−(c) correspond to $\phi = 0, \pi/2, \pi$, respectively.

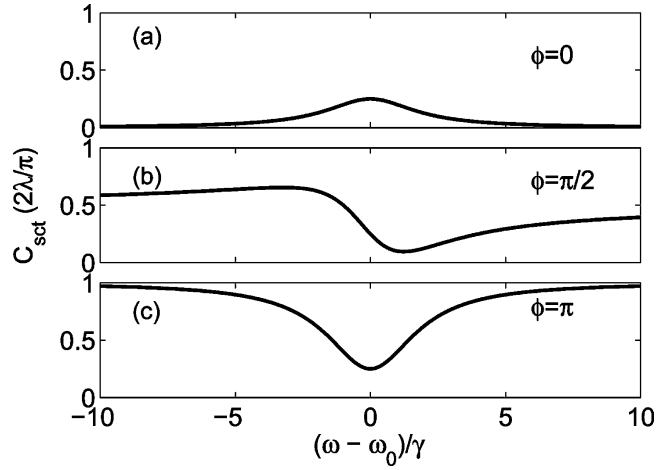

Figure 2. Scattering cross-section spectrum as given by eq 23 for the lossy case with $\gamma_0 = \gamma$.

For all cases where ϕ is not equal to 0 or π, the spectrum is not a Lorentzian but rather exhibits a Fano asymmetric line shape, which exhibits both enhancement and suppression of scattering coefficients in the vicinity of the resonance. For example, Figure 1b shows the scattering cross-section spectrum for $\phi = \pi/2$. We note that in the Fano line shape, neither the minimum nor the maximum in scattering cross-section occurs at the resonant frequency ω_0. Through eq 23a, we can determine that the minimum and maximum occur at the frequency $\omega_0 \pm \gamma \tan(\phi/2)$ and $\omega_0 \mp \gamma \cot(\phi/2)$ respectively, where the $\pm$ sign corresponds to $0 < \phi < \pi$ or $-\pi < \phi < 0$. Therefore, to switch the scattering cross-section from the minimum to the maximum, the smallest frequency required is 2γ, which is for the case $\phi = \pm\pi/2$. This result is in fact consistent with a previous study on optical switching using Fano resonances.[20]

When $\phi = \pi$, the background exhibits maximum scattering, and the presence of the resonance creates a dip at ω_0; no scattering occurs at the resonance frequency (Figure 1c). This effect is closely related to the all-optical analogue of EIT, which occurs when a super-radiant state has the same resonant frequency as a subradiant state in the same scattering channel. The super-radiant state by itself establishes a broad scattering peak and thus can be regarded as establishing a background in

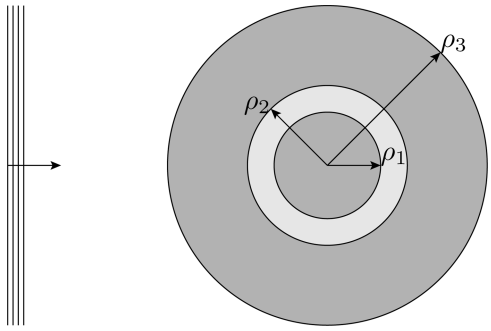

Figure 3. Schematic of a metal−dielectric−metal cylinder obstacle. The dark gray area is a metal described by a Drude model. The light gray area is dielectric ($\varepsilon_d = 12.96$). The surrounding media is assumed as air.

the vicinity of the subradiant resonance. The presence of the subradiant state introduces a dip and renders the system transparent (i.e., with zero scattering) at the resonant frequency. A better treatment of the EIT effect, however, requires one to treat the super-radiant and the subradiant state at an equal footing[21] and will be done in later works.

To show the effect of the intrinsic loss, Figure 2 shows the scattering cross-section spectra when $\gamma_0 = \gamma$. Comparing it to Figure 1, one can see that the line shapes are similar to the corresponding lossless cases, but the presence of the loss reduces the cross-section variation as a function of frequency. In particular, the scattering cross-section can no longer reach $2\lambda/\pi$, which is the maximal contribution possible in a single channel. Neither can the scattering cross-section reach zero. In the presence of loss it is no longer possible to completely eliminate the scattering effect at a single frequency through the use of a Fano interference with a single resonance.

We now consider the absorption cross-section spectrum described by eq 23b. In contrast to the scattering cross-section spectrum, which varies with the background phase factor, the absorption cross-section is independent of the phase factor. Instead, it always has a symmetric Lorentzian line shape with its maximum at the resonant frequency. Thus, Fano interference effect does not affect the absorption properties of the obstacle.

III. Numerical Validation

To check the validity of the above theory, we compare eq 23 to the results of numerical simulations based on the Lorentz−Mie method of a cylindrical scatterer. Figure 3 shows the schematic of the scatterer, which consists of multiple concentric layers of metal and a dielectric. The permittivity of the dielectric is $\varepsilon_d = 12.96$, and the metal is described by a Drude model $\varepsilon_m = 1 - \omega_p^2/(\omega^2 + i\gamma_d\omega)$ (ω_p and γ_d are the plasma frequency and the damping rate, respectively). In the frequency range $\omega < \omega_p$, a corresponding planar structure can support surface-plasmon waveguide modes that are confined in the dielectric region. For the cylindrical structure, whispering gallery modes related to such waveguide modes can be formed in the low angular momentum channels.[22]

We start with the lossless case where $\gamma_d = 0$. For the geometry parameters of $\rho_1 = 0.285\lambda_p$, $\rho_2 = \lambda_p$, and $\rho_3 = 1.5\lambda_p$ (where $\lambda_p = 2\pi c/\omega_p$, with c being the speed of light in vacuum), the scattering cross-section for the $l = 0$ channel is plotted as circles in Figure 4a. It shows a typical Fano resonant line shape around $0.155\omega_p$.

To compare to the analytic results, we determine the parameters required in eq 23 in the following way: We express the H field in each layer as a linear superposition of $J_0(k\rho)$ and $H_0^{(1)}(k\rho)$, except in the innermost layer where the field is proportional to only J_0 and the outermost layer where the field is proportional to only $H_0^{(1)}$. By matching the boundary condition at all metal−dielectric interfaces, we obtain a transcendental equation with frequency as a variable. By solving for the complex roots of the transcendental equation, we determine the resonance frequency (the real part of the root) and the leakage rate (the imaginary part of the root). For the structure shown here, in the lossless case, we obtain $\omega_0 = 0.1552\omega_p$, $\gamma = 1.9166 \times 10^{-5}\omega_p$. The phase factor $\phi = -0.4882\pi$ is established by calculating the scattering coefficient of a uniform metallic cylinder with the same size. Using these parameters, the

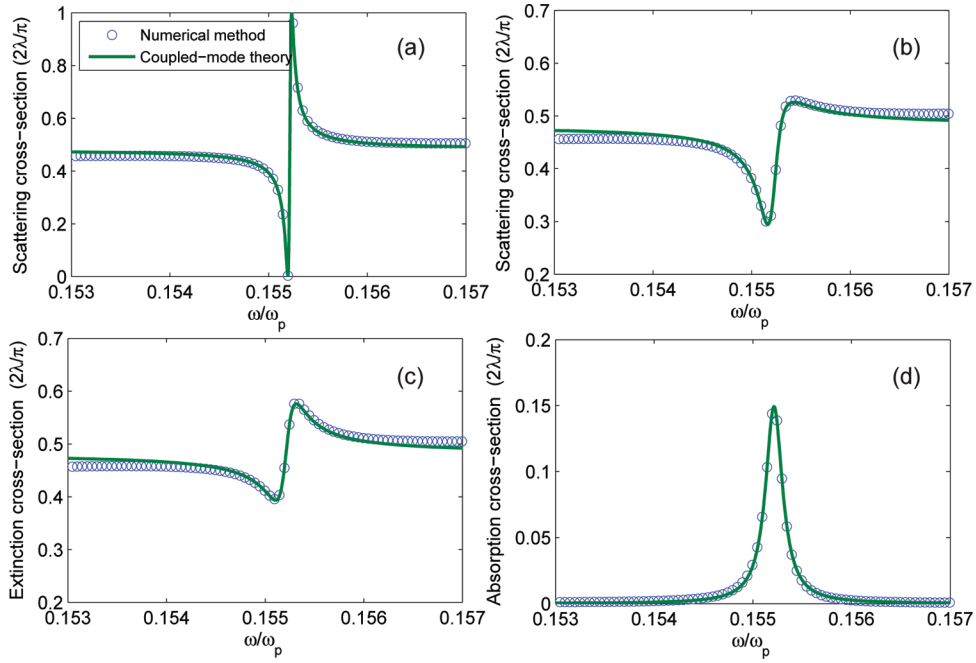

Figure 4. Cross-section of the $l = 0$ channel for the scatterer shown in Figure 3, where the geometric parameters are $\rho_1 = 0.285\lambda_p$, $\rho_2 = \lambda_p$, and $\rho_3 = 1.5\lambda_p$ (λ_p is the wavelength in the vacuum at the plasma frequency ω_p): (a) scattering cross-section for the lossless metal case of $\gamma_d = 0$; (b)−(d) the scattering, extinction, and absorption cross-section spectra for the lossy metal case of $\gamma_d = 0.001\omega_p$.

scattering cross-section calculated by eq 23a shows an excellent agreement with the numerical result (Figure 4a).

We now introduce a metal loss characterized by $\gamma_d = 0.001\omega_p$. Repeating the same process as outlined above for the lossless case, we determine a resonant frequency $\omega_0 = 0.1552\omega_p$ and a total loss rate $\gamma + \gamma_0 = 1.0492 \times 10^{-4}\omega_p$. Assuming that the leakage rate is the same as the lossless case, i.e., $\gamma = 1.9166 \times 10^{-5}\omega_p$, we have the intrinsic loss rate $\gamma_0 = 8.5749 \times 10^{-5}\omega_p$. The background phase shift ϕ is determined using the same procedure by considering the scattering of a corresponding uniform metallic cylinder, which results in $\phi = -0.4882\pi + 8.6 \times 10^{-4}$i. Comparing with the lossless case, we notice that the background phase shift is not significantly affected by introducing loss in the system. Thus, in the theory for the lossy case, we will choose as a parameter the background phase shift $\phi = -0.4882\pi$, and ignore the small loss that occurs in the background. Using these parameters, the theoretical spectra again agree well with the numerical spectra (Figure 4b−d). The example here thus provides a validation of the theory in the single channel case.

IV. Multiple-Channel Resonant Obstacle

The theory developed in section II can be straightforwardly generalized to include resonances in multiple channels (where the resonance in each channel can only be excited by the same channel incoming wave and coupled to the same channel outgoing wave), since the total cross-section is the sum of the contributions from all channels. As an example, here we apply our theory to a metal−dielectric−metal cylinder scatterer where all channels that strongly contribute to the scattering process exhibit the Fano effect.

We again consider the structure shown in Figure 3, with a new set of parameters $\rho_1 = 0.36\lambda_p$, $\rho_2 = 0.73\lambda_p$, and $\rho_3 = \lambda_p$. The metal has a damping rate $\gamma_d = 0.001\omega_p$. The circles in Figure 5a,b correspond to the scattering and absorption cross-section spectra, respectively, as obtained from numerical simulations. In the frequency range $0.22-0.233\omega_p$, the total cross-section of the system is dominated by the contributions from five channels of $l = 0, \pm1, \pm2$. For each channel, the scattering cross-section spectrum and the absorption cross-section spectrum show the Fano and Lorentzian line shapes, respectively. We use the above theory to fit these curves. The fitting results are plotted as the solid lines in Figure 5, which again indicates good agreement between theory and simulation.

We note that this obstacle can be potentially used as a cloaked sensor[23]—when the obstacle is placed in an electromagnetic field, it absorbs the energy but creating only minimum scattering within a narrow range of frequencies. From Figure 5, one can see that at the frequency $\omega = 0.2282\omega_p$, the total scattering cross-section of the obstacle is only $0.03(2\lambda/\pi)$, while the total absorption cross-section is $0.32(2\lambda/\pi)$. In the presence of loss, the scattering of the particle cannot be completely eliminated in this case, as can be seen from eq 21. Nevertheless, the scattering can be substantially reduced as we show here. The Fano interference effect thus provides an interesting alternative mechanism for creating a cloaked sensor as compared to ref 23.

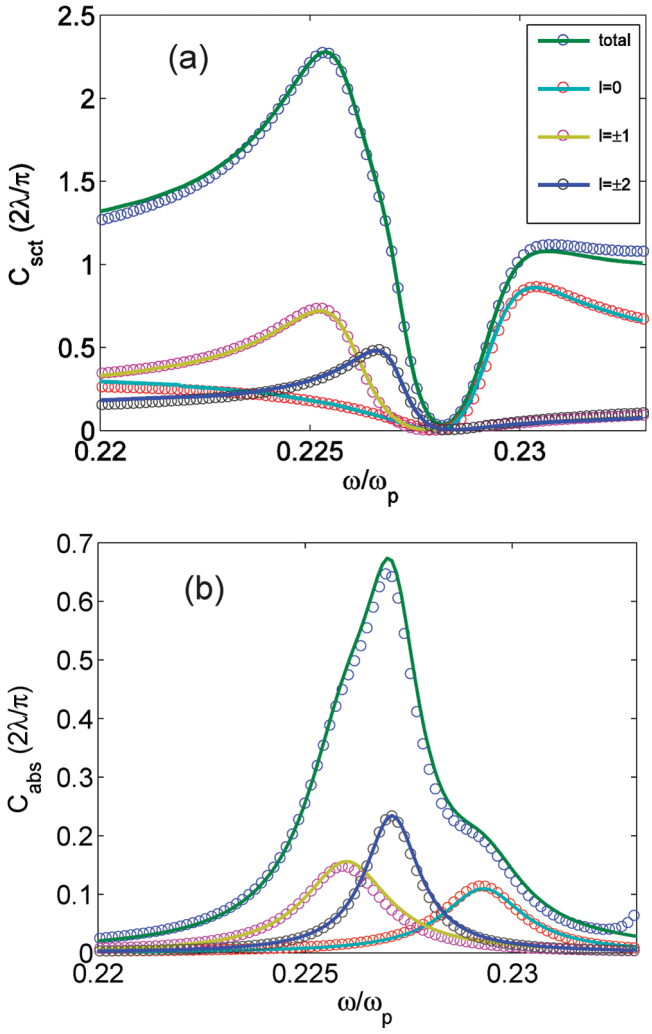

Figure 5. Scattering (a) and absorption (b) cross-section spectra for the scatterer shown in Figure 3, with the geometric parameters of $\rho_1 = 0.36\lambda_p$, $\rho_2 = 0.73\lambda_p$, and $\rho_3 = \lambda_p$, and the metal damping rate of $\gamma_d = 0.001\omega_p$. The circles are from the Lorentz−Mie method, and the solid lines are the theoretical fit using eq 23.

V. Summary and Outlook

In summary, we present a theory for Fano interference in light scattering by individual obstacle, based on a temporal coupled-mode formalism. We show that for each angle momentum channel, the Fano interference effect can be modeled by a simple temporal coupled-mode equation, which provides a line shape formula for scattering and absorption cross-section. We validate the analysis with numerical simulations. As an application, we design a structure that exhibits strong absorption and at the same time weak scattering properties.

We note that this theory is applicable for obstacles that are much smaller than the incident wavelength, or systems that have two-dimensional cylindrical or three-dimensional spherical symmetry. For arbitrary-shaped obstacles or assembled clusters, the overall scattering matrix of the system is no longer diagonalizable in the angular momentum basis. Instead, for a theory of Fano interference, one may define the channel as the eigenstates of the background scattering matrix, the resonance in this case is likely then to couple to several scattering channels simultaneously. Such a theory will be developed in future research.

Acknowledgment. This work is supported by DARPA/MARCO under the Interconnect Focus Center, by AFOSR Grant No. FA9550-04-1-0437, and by the DOE Grant No. DE-FG 07ER46426.

References and Notes

(1) Bohren, C.; Huffman, D. *Absorption and Scattering of Light by Small Particles*; John Wiley & Sons Inc.: New York, 1983.

(2) Fano, U. *Phys. Rev.* **1961**, *124*, 1866.
(3) Tribelsky, M. I.; Flach, S.; Miroshnichenko, A. E.; Gorbach, A. V.; Kivshar, Y. S. *Phys. Rev. Lett.* **2008**, *100*, 043903.
(4) Fedotov, V. A.; Rose, M.; Prosvirnin, S. L.; Papasimakis, N.; Zheludev, N. I. *Phys. Rev. Lett.* **2007**, *99*, 147401.
(5) Luk'yanchuk, B. S.; Tribelsky, M. I.; Ternovsky, V.; Wang, Z. B.; Hong, M. H.; Shi, L. P.; Chong, T. C. *J. Opt. A: Pure Appl. Opt.* **2007**, *9*, S294.
(6) Christ, A.; Martin, O. J. F.; Ekinci, Y.; Gippius, N. A.; Tikhodeev, S. G. *Nano Lett.* **2008**, *8*, 2171.
(7) Liu, N.; Kaiser, S.; Giessen, H. *Adv. Mater.* **2008**, *20*, 4521.
(8) Hao, F.; Sonnefraud, Y.; Van Dorpe, P.; Maier, S. A.; Halas, N. J.; Nordlander, P. *Nano Lett.* **2008**, *8*, 3983.
(9) Harris, S. E. *Phys. Today* **1997**, *50*, 36.
(10) Zhang, S.; Genov, D. A.; Wang, Y.; Liu, M.; Zhang, X. *Phys. Rev. Lett.* **2008**, *101*, 047401.
(11) Tassin, P.; Zhang, L.; Koschny, T.; Economou, E. N.; Soukoulis, C. M. *Phys. Rev. Lett.* **2009**, *102*, 053901.
(12) Yannopapas, V.; Paspalakis, E.; Vitanov, N. V. *Phys. Rev. B* **2009**, *80*, 035104.
(13) Tassin, P.; Zhang, L.; Koschny, T.; Economou, E. N.; Soukoulis, C. M. *Opt. Express* **2009**, *17*, 5595.
(14) Papasimakis, N.; Fedotov, V.; Zheludev, N.; Prosvirnin, S. *Phys. Rev. Lett.* **2008**, *101*, 253903.
(15) Papasimakis, N.; Fu, Y. H.; Fedotov, V. A.; Prosvirnin, S. L.; Tsai, D. P.; Zheludev, N. I. *Appl. Phys. Lett.* **2009**, *94*, 211902.
(16) Liu, N.; Langguth, L.; Weiss, T.; Kästel, J.; Fleischhauer, M.; Pfau, T.; Giessen, H. *Nat. Mater.* **2009**, *8*, 758.
(17) Fan, S.; Suh, W.; Joannopoulos, J. D. *J. Opt. Soc. Am. A* **2003**, *20*, 569.
(18) Hamam, R. E.; Karalis, A.; Joannopoulos, J. D.; Soljačić, M. *Phys. Rev. A* **2007**, *75*, 53801.
(19) Haus, H. *Waves and Fields in Optoelectronics*; Prentice-Hall: Englewood Cliffs, NJ, 1984.
(20) Fan, S. *Appl. Phys. Lett.* **2002**, *80*, 908.
(21) Suh, W.; Wang, Z.; Fan, S. *IEEE J. Quantum Electron.* **2004**, *40*, 1511.
(22) Catrysse, P. B.; Fan, S. *Appl. Phys. Lett.* **2009**, *94*, 231111.
(23) Alù, A.; Engheta, N. *Phys. Rev. Lett.* **2009**, *102*, 233901.

JP9089722